BNL-113404-2017-JA

Improving the radiation hardness of graphene field effect transistors

Konstantinos Alexandrou, Amrita Masurkar, Hassan Edrees, James F. Wishart, Yufeng Hao, Nicholas Petrone, James Hone, Ioannis Kymissis

Submitted to Applied Physics Letters

October 2016

Chemistry Department

Brookhaven National Laboratory

U.S. Department of Energy
USDOE Office of Science (SC),
Basic Energy Sciences (BES) (SC-22)

DISCLAIMER

Improving the Radiation Hardness of Graphene Field Effect Transistors

Konstantinos Alexandrou[1, a)], Amrita Masurkar[1], Hassan Edrees[1], James F. Wishart[3], Yufeng Hao[2], Nicholas Petrone[2], James Hone[2], Ioannis Kymissis[1*]

[1)]Department of Electrical Engineering Columbia University, New York, 10027, United States

[2)]Department of Mechanical Engineering, Columbia University, New York, 10027, United States

[3)]Chemistry Division, Brookhaven National Laboratory, Upton, New York, 11973- 5000, United States

ABSTRACT

Ionizing radiation poses a significant challenge to the operation and reliability of conventional silicon-based devices. Here, we report the effects of gamma radiation on graphene field-effect transistors (GFETs), along with a method to mitigate those effects by developing a radiation-hardened version of our back-gated GFETs. We demonstrate that activated atmospheric oxygen from the gamma ray interaction with air damages the semiconductor device, and damage to the substrate contributes additional threshold voltage instability. Our radiation-hardened devices, which have protection against these two effects, exhibit minimal performance degradation, improved stability, and significantly reduced hysteresis after prolonged gamma radiation exposure. We believe this work provides an insight on graphene's interactions with ionizing radiation that could enable future graphene-based electronic devices to be used for space, military, and other radiation-sensitive applications.

[a)] kka2114@columbia.edu

Graphene-based devices, with their unique electrical,[1-3] mechanical,[4] and optical properties,[5] demonstrate a huge potential for future technological applications. Different challenges arise when these devices have to operate in a radiation harsh environment.[6-8] Undesirable phenomena that silicon-based devices are prone to such as total dose effects, single event upsets, displacement damage and soft errors,[9-10] can have a detrimental impact on performance and reliability. Similarly, the significant effects of irradiation on carbon nanotubes[11-13] indicate the potential for related radiation-induced defects in carbon-based materials such as graphene.

The GFET is a convenient vehicle with which to investigate the effects of gamma radiation at the material and device levels. A number of investigators have examined the effect of radiation on GFETs and have shown that despite graphene's low thickness and low nominal cross-section, the material exhibits high susceptibility to radiation-induced effects. Graphene's field-effect mobility and charge neutrality (Dirac) point are particularly sensitive to unintentional doping from the surrounding environment,[14] and traps and fixed charges at the substrate/oxide interface can negatively affect GFET performance.[15,16] Gamma radiation has a significant impact on GFET performance[17] and prior studies have shown that it can create electrically active defects in substrates and additionally increase the trap density between interfaces.[18,19] Graphene can also be used as a radiation sensor,[20] in which the detection mechanism relies on the sensitivity of graphene's resistivity to local electric field changes caused by radiation induced ionized charges in the underlying substrate. Gamma radiation and displacement damage have been shown to have an effect on graphene's lattice structure,[21] while Raman spectroscopy has shown p-doped behavior in irradiated graphene.[22] In addition, encapsulated hBN graphene devices have been

tested under X-Ray irradiation, highlighting the effect of boron nitride in mitigating radiation effects.[23] This body of work demonstrates not only the mechanisms of ionized charge build up in the substrate and displacement damage effects on GFET performance, but also that atmospheric adsorbents from the surrounding environment can have a significant impact on the radiation hardness of graphene.

In our study we examined three device configurations to separate the effect of atmospheric and substrate effects. A non-encapsulated back-gated device topology (Figure 1 (a) (iv)) based on a heavily-doped Si/SiO_2 substrate is exposed to all effects, an encapsulated GFET structure which uses a Parylene-C/aluminum encapsulation layer[28] (Figure 1 (c)) protects against atmospheric effects, and a device that combines both encapsulation and a buried aluminum gate providing shielding against both effects (Figure 1 (d)).

Back-gated GFETs were fabricated using single-layer graphene grown by chemical vapor deposition[24] (CVD) on 25 um copper foils and transferred on top of 300 nm of thermally grown oxide on p-doped Si substrates. Our mechanical transfer method was based[25] on a spin-coated thin layer of poly(methyl methacrylate) (PMMA) acting as a supporting layer where we add an additional polydimethylsiloxane (PDMS) stamp on top for extra support as shown in Figure 1 (a). Trapped water while transferring has been demonstrated to significantly contribute to the p-doping of graphene.[26] The use of PDMS allows us to leave the graphene/PMMA/PDMS stack to dry for 24 hours, reducing trapped water at the graphene/SiO_2 interface. The absence of a D-peak in the Raman spectrum in Figure 1 (b) shows the high crystalline quality of the CVD-graphene, and the I_{2D}/I_G intensity ratio of more than three clearly confirms the monolayer nature of the transferred layer.[27]

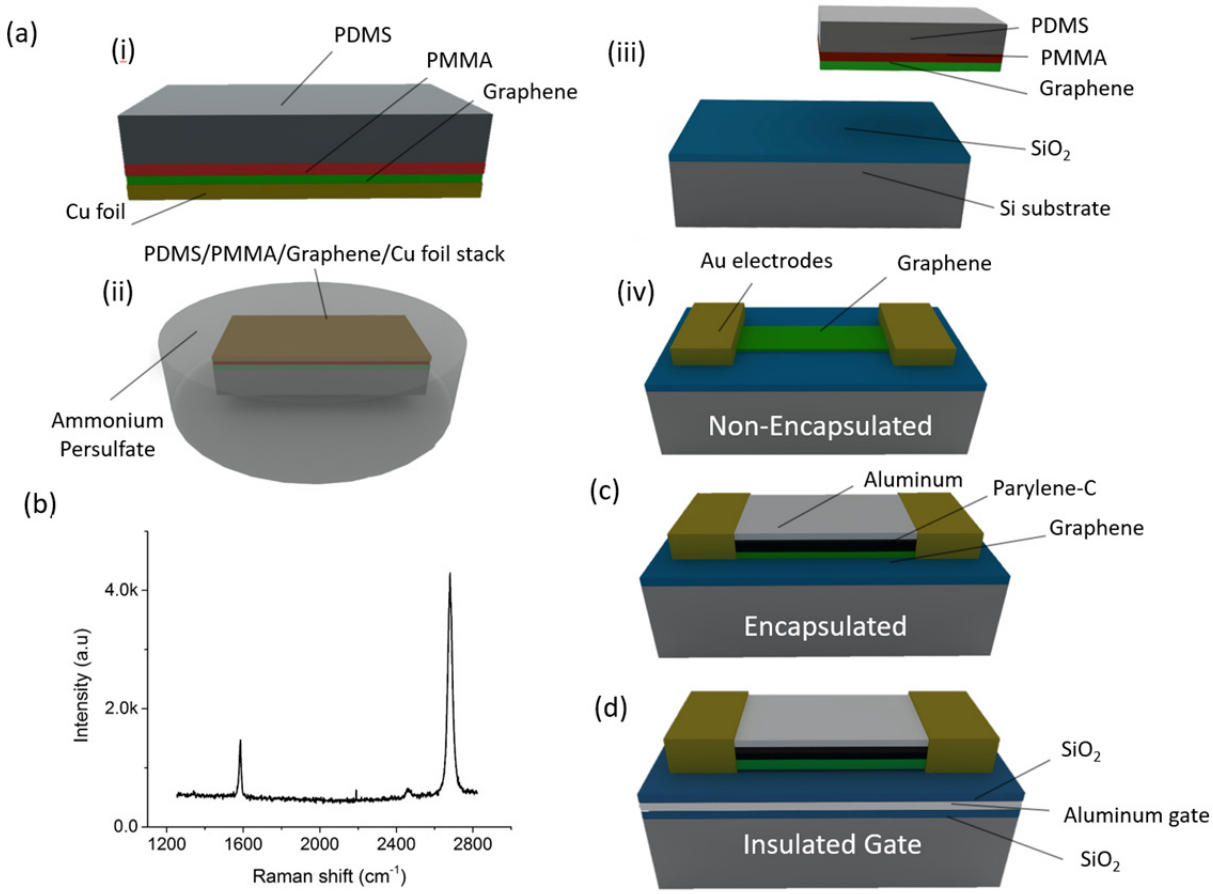

FIG. 1. (a) GFET fabrication process. (b) Raman spectra of single-layer graphene (SLG) on a Si/SiO_2 substrate. (c) Encapsulated graphene device structure based on a 1.25 um Parylene-C and 50 nm aluminum layer. (d) Insulated gate structure with a 50 nm aluminum back-gate electrode and same passivation layer as the one presented in (c).

Transfer curves of the non-encapsulated devices (Figure 1 (a) (iv)) irradiated with various doses in ambient environment are shown in Figure 2 (a). For the gamma irradiation we used a ^{60}Co source at the Chemistry Department of Brookhaven National Laboratory. The dose rate was approximately 1 kGy/hr (due to the 5.26-year half-life of ^{60}Co, the dose rate decreased slightly over the course of these experiments), and comparable to doses that electronics are exposed in multiyear space missions.[37] Field-effect mobilities (μ_{FE}) were extracted from measured I_d-V_{gs} characteristics by using the following equation: $\mu_{FE}=L_{ch}\, g_m / (W_{ch}\, C_G V_{gs})$, where L_{ch} and W_{ch} are the length and width of the GFET channel, g_m is the terminal transconductance, C_g is the gate

capacitance and V_{gs} is the applied gate/source voltage. The Dirac point of each device was obtained in order to identify any possible effects of irradiation on overall performance and doping profile.[29]

After 2.2 kGy of gamma irradiation, the GFET exhibits a slight change in μ_{FE}, as shown in Figure 2 (a), where the μ_{FE} of the as-fabricated device decreases by 13.7%. At the same time, the Dirac point shifts toward higher back-gate bias by 12 V, indicating an increased p-doped behavior of the device. In addition, non-encapsulated devices that were subjected to 26.4 kGy of irradiation as shown in the inset of Figure 2 (a), exhibit a larger decrease in μ_{FE} (30.53% decrease) and a higher ΔV_{Dirac} of 20 V compared to devices that were subjected to 2.2 kGy.

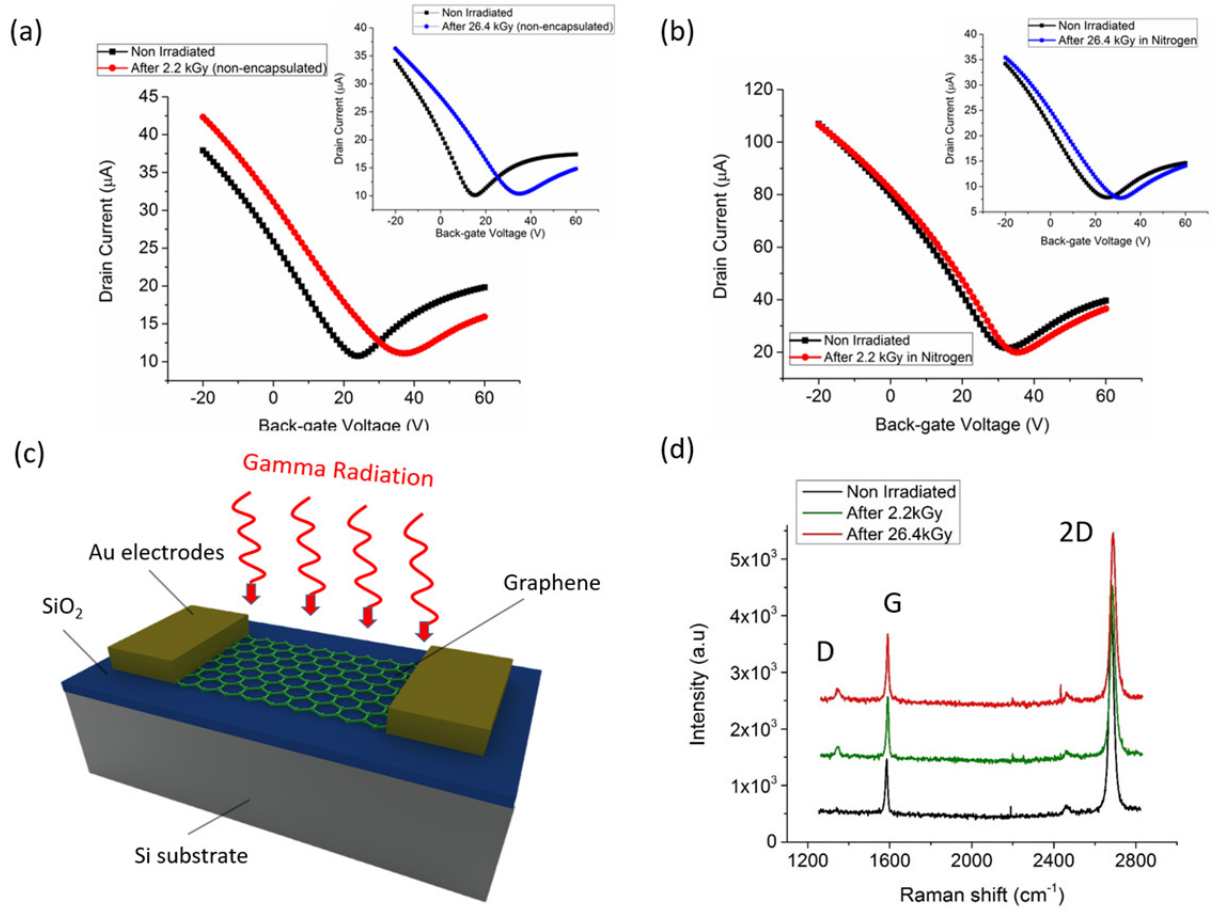

FIG. 2. (a) Transfer characteristics for non-encapsulated GFETs irradiated with 2.2 kGy (a) and 26.4 kGy (inset). (b) Transfer characteristics of GFETs irradiated with 2.2 kGy (b) and 26.4kGy (inset) in nitrogen filled environment (c) Schematic illustration of the device exposed to gamma rays **(d)** Raman spectrum of the irradiated devices

Figure 2 (d) shows Raman spectra analysis of non-irradiated and irradiated devices subjected to 2.2 kGy and 26.4 kGy. Our primary focus is the ratio of D band (~1350cm^{-1}) to G band (~1580-1600 cm^{-1}) (I_D/I_G), as it is a measure of the degree of disorder of single layer graphene (SLG).[30] Non-irradiated graphene samples have I_D/I_G=0.03, whereas the samples irradiated with 2.2 kGy and 26.4 kGy of gamma rays have I_D/I_G=0.165 and I_D/I_G=0.182, respectively. This increase in I_D/I_G can be attributed to possible displacement damage on the graphene lattice that can lead to vacancies or local structural defects through the Compton effect as previous reports have found.[8] As the G band position is sensitive to chemical doping because of the strong electron – phonon interaction in graphene,[31] any noticeable increase due to irradiation can provide valuable information concerning the doping profile of our samples. The G-band exhibited a 4.93 cm^{-1} shift towards higher wavenumbers after samples were exposed to 2.2 kGy of gamma radiation and a further 1.02 cm^{-1} shift when tested under 26.4 kGy, substantiating the increase in p-doping, in good agreement with the transport data.

X-ray Photoelectron Spectroscopy (XPS) was employed to further investigate the effects of the ambient environment on the non-encapsulated irradiated devices. XPS spectra were collected using a Phi system with a standard Mg Kα source and spot size of ~100 microns. In Figure 3 (a), C1s XPS data from three different device configurations are presented and peaks were fit using a Gaussian-Lorentzian blend. The data are comprised of four peaks positioned at ~284.5 eV, ~285.2 eV, ~286.4 eV, and ~288.6 eV, corresponding to C-C, C-OH, C-O-C, and -COOH bonds, respectively. Table 1 shows the percent area that each peak makes up of the total C1s spectral area. UV-ozone exposed graphene suffers from high oxygen adsorption and

doping,[32] while others have shown that gamma radiation induces ozone formation in air.[33] For these reasons, a UV-ozone treated sample was included in our XPS measurements, to compare its oxygen content to that of the gamma irradiated sample. Both UV-ozone and 26.4 kGy gamma radiation treatment show similar trends. The main carbon peak decreases, while the C-OH, C-O-C and -COOH peaks increase in area. These results clearly indicate that gamma irradiation increases the adsorption of oxygen resulting in degraded electronic performance. A passivation layer is therefore crucial to isolate the graphene channel from oxygen if these devices are to operate with stable properties in a radiation sensitive environment.

Table 1| XPS C1s bond area

	No Irradiation Bond Area %	**UV-Ozone Bond Area %**	**26.4 kGy Bond Area %**
C-C	66.4	40.0	46.8
C-OH	16.4	38.4	27.7
C-O-C	9.7	7.6	15.3
-COOH	7.5	14.0	10.2

To further investigate the role of the ambient environment during irradiation, we performed exposures of non-encapsulated devices in a nitrogen environment to eliminate any oxygen/ozone contribution that we previously observed. Samples were sealed inside N_2-filled tubes and subsequently irradiated with 2.2 kGy and 26.4 kGy gamma rays under the same conditions as before. Results from Figure 2 (b) show a substantial improvement of the irradiated devices in a N_2 environment when compared to the air exposed devices. Specifically, GFETs shown in Figure 2 (b) exhibit a ΔV_{Dirac} of 2 V and a μ_{FE} decrease of 0.84% after 2.2 kGy of

irradiation, whereas GFETs irradiated under the same conditions in an air environment (Figure 2 (a)) exhibit a ΔV_{Dirac} of 12 V and a μ_{FE} decrease of 13.7%. Similarly, devices exposed to 26.4 kGy of radiation had a ΔV_{Dirac} of 6 V and a μ_{FE} decrease of 5.61% in N_2 atmosphere (inset of Figure 2 (b)) while a ΔV_{Dirac} of 20 V and a μ_{FE} decrease of 30.5% was observed in ambient air (inset of Figure 2 (a)).

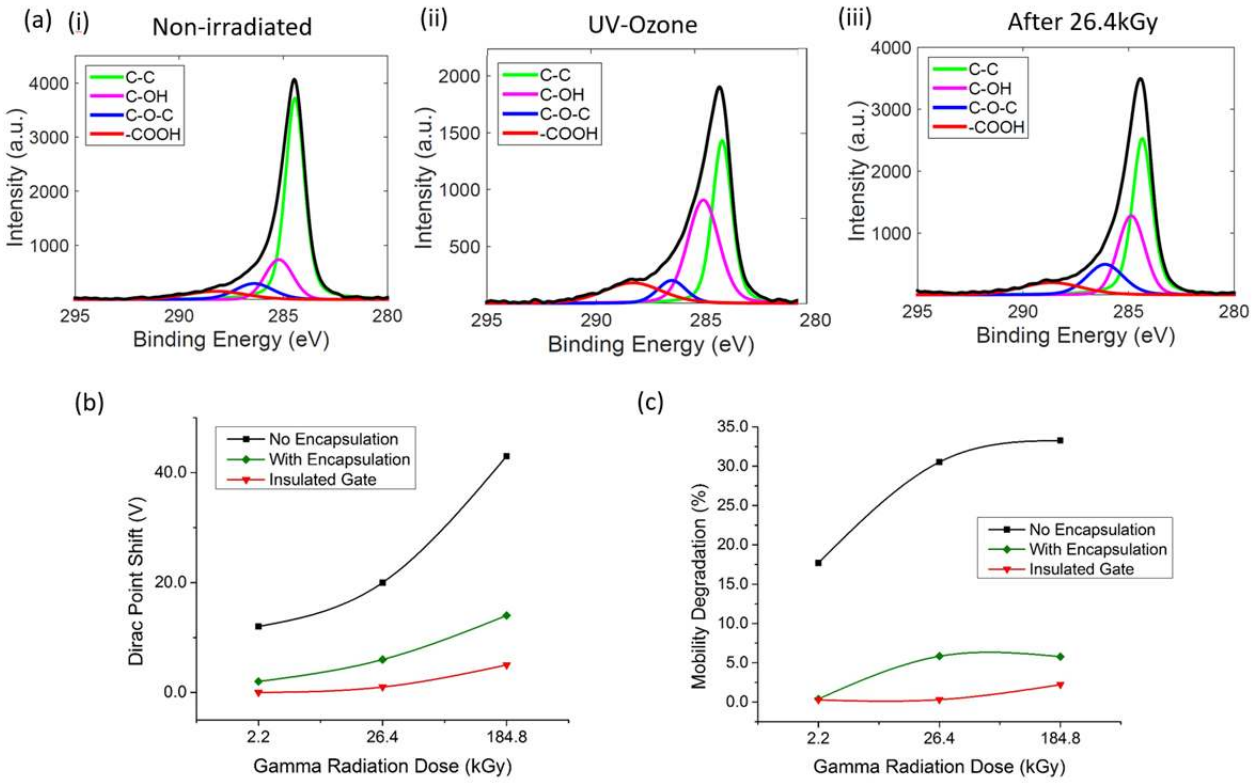

FIG. 3. (a) Carbon 1s XPS data from three different devices: non-irradiated (i), UV-ozone treated samples (ii) and after 26.4 kGy gamma rays (iii). (b), (c) V_{Dirac} shift and mobility degradation (%) results for all three device structures irradiated in air environment.

Based on the results from our XPS and N_2 measurements, we developed an encapsulation method for GFETs in order to shield graphene from the surrounding environment while being irradiated. Our encapsulation method is based on the deposition of 1.25 um Parylene-C and 50 nm aluminum layers on top of the exposed graphene channel as shown in Figure 1 (c), and has already enabled our devices to operate for several weeks in ambient environment with minimal

performance degradation.[28] In addition, the combination of Parylene-C and aluminum has been proven to be an effective encapsulation method as it provides a water/moisture barrier and air stability to organic semiconductors.[34]

Encapsulated GFETs were subjected to the same irradiation conditions as before, and as Figures 3 (b), (c) show, they perform significantly better when compared to the non-encapsulated devices. Specifically, non-encapsulated devices demonstrate a ΔV_{Dirac} up to 43 V when irradiated with 184.8 kGy, while the V_{Dirac} of encapsulated devices shifts only 14 V. In addition, μ_{FE} of the non-encapsulated GFETs was severely affected with a decrease up to 33.2% when the encapsulated devices only lost 5.7% compared to the as-fabricated μ_{FE} values. These results clearly highlight the effectiveness of the encapsulation layer as a barrier to oxygen and ozone.

Besides displacement damage and ambient environment contributions, radiation-induced defects in the substrate and substrate/oxide interface can have a significant effect on device performance. Carrier lifetimes, mobilities and carrier densities can be negatively affected as energy deposited by radiation creates electrically active defects in the substrate.[10] These radiation mechanisms may further affect our non-encapsulated and encapsulated devices since they both use silicon as a back-gate electrode. For this reason, we developed an insulated gate structure in which the buried Al layer was used as a back-gate electrode.

Figure 1 (d) shows our insulated gate GFET device structure, where a 50 nm aluminum gate was thermally evaporated on top of the Si/SiO_2 substrate, followed by a 100 nm SiO_2 gate oxide film using plasma enhanced chemical vapor deposition (PECVD). The previously used Parylene-C/aluminum encapsulation was also used on the insulated gate design and devices were

tested under exactly the same conditions as before. Prior to irradiation, the insulated gate GFET exhibits similar electrical performance and stability to the encapsulated structure, with a V_{Dirac} of 20 V and μ_{FE} of 650 cm^2/Vs. Figure 3 (b) shows that irradiation can cause a ΔV_{Dirac} of up to 5 V to the insulated gate devices, a substantial improvement over the encapsulated devices used before (Figure 1 (c)) which exhibited a ΔV_{Dirac} of up to 14 V under the same irradiation conditions. In addition, the μ_{FE} of the insulated gate devices as shown in Figure 3 (c), decreased by only 2% after irradiation, whereas encapsulated devices suffered from a 6% decrease in μ_{FE}.

Radiation harsh environments pose a significant challenge to the performance and reliability of next generation graphene-based devices. In this work, we studied the effects of gamma radiation on GFETs and developed a method to shield them. The ambient environment, radiation induced defects to the substrate, and displacement damage are three main factors contributing to GFET performance degradation. We demonstrate that both encapsulation and an insulated gate are needed to effectively produce radiation-hard GFETs. Our proposed encapsulation and gate insulation structures mitigate gamma radiation effects, paving the way for the use of graphene-based electronics in radiation-sensitive environments. Finally, our shielding method may be advantageous to other types of radiation (such as electrons or ions) as well, since these devices exhibit similar degradation mechanisms to our gamma study.[35-36]

ACKNOWLEDGMENTS

This material is based upon work supported by the NSF MRSEC program through Columbia in the Center for Precision Assembly of Superstratic and Superatomic Solids (DMR-1420634) and the Defense Threat Reduction Agency (DTRA) under HDTRA1-11-0022. The work at BNL and use of the ^{60}Co source of the BNL Accelerator Center for Energy Research were supported by

the US-DOE Office of Science, Division of Chemical Sciences, Geosciences and Biosciences under contracts DE-AC02-98CH10886 and DE-SC0012704.

REFERENCES

(1) K. Novoselov, Science 306, (2004).

(2) Y. Zhang, Y. Tan, H. Stormer and P. Kim, Nature 438, (2005).

(3) A. Geim and K. Novoselov, Nature Materials 6, (2007).

(4) C. Lee, X. Wei, J. Kysar and J. Hone, Science 321, (2008).

(5) R. Nair, P. Blake, A. Grigorenko, K. Novoselov, T. Booth, T. Stauber, N. Peres and A. Geim, Science 320, (2008).

(6) A. Hashimoto, K. Suenaga, A. Gloter, K. Urita and S. Iijima, Nature 430, (2004).

(7) D. Teweldebrhan and A. Balandin, Appl. Phys. Lett. 94, (2009).

(8) Y. Wang, Y. Feng, F. Mo, G. Qian, Y. Chen, D. Yu, Y. Wang and X. Zhang, Appl. Phys. Lett. 105, (2014).

(9) E. Stassinopoulos and J. Raymond, Proceedings Of The IEEE 76, (1988).

(10) J. Srour, C. Marshall and P. Marshall, IEEE Trans. Nucl. Sci. 50, (2003).

(11) F. Banhart, Rep. Prog. Phys. 62, (1999).

(12) C. Cress, J. McMorrow, J. Robinson, A. Friedman, H. Hughes, B. Weaver and B. Landi, MRC 1, (2011).

(13) C. Cress, J. McMorrow, J. Robinson, B. Landi, S. Hubbard and S. Messenger, Electronics 1, (2012).

(14) C. Aguirre, P. Levesque, M. Paillet, F. Lapointe, B. St-Antoine, P. Desjardins and R. Martel, Adv. Mater. 21, (2009).

(15) H. Wang, Y. Wu, C. Cong, J. Shang and T. Yu, ACS Nano 4, (2010).

(16) C. Dean, A. Young, I. Meric, C. Lee, L. Wang, S. Sorgenfrei, K. Watanabe, T. Taniguchi, P. Kim, K. Shepard and J. Hone, Nature Nanotech 5, (2010).

17) K. Alexandrou, A. Masurkar, H. Edrees, J. F. Wishart, Y. Hao, N. Petrone, J. Hone and I. Kymissis, Device Research Conference, (2016)

18) E. Zhang, A. Newaz, B. Wang, S. Bhandaru, C. Zhang, D. Fleetwood, K. Bolotin, S. Pantelides, M. Alles, R. Schrimpf, S. Weiss, R. Reed and R. Weller, IEEE Trans. Nucl. Sci. 58, (2011).

19) C. Cress, J. Champlain, I. Esqueda, J. Robinson, A. Friedman and J. McMorrow, IEEE Trans. Nucl. Sci. 59, (2012).

(20) A. Patil, O. Koybasi, G. Lopez, M. Foxe, I. Childres, C. Roecker, J. Boguski, J. Gu, M.L. Bolen, M.A. Capano et al. (NSS/MIC), IEEE, pp. 455-459, (2011)

(21) A. Ansón-Casaos, J. Puértolas, F. Pascual, J. Hernández-Ferrer, P. Castell, A. Benito, W. Maser and M. Martínez, Applied Surface Science 301, (2014).

(22) D. Kleut, Z. Marković, I. Holclajtner Antunović, M. Dramićanin, D. Kepić and B. Todorović Marković, Phys. Scr. T162, (2014).

23) C. Zhang, B. Wang, G. Duan, E. Zhang, D. Fleetwood, M. Alles, R. Schrimpf, A. Rooney, E. Khestanova, G. Auton, R. Gorbachev, S. Haigh and S. Pantelides, IEEE Trans. Nucl. Sci. 61, (2014).

(24) Y. Hao, M. Bharathi, L. Wang, Y. Liu, H. Chen, S. Nie, X. Wang, H. Chou, C. Tan, B. Fallahazad, H. Ramanarayan, C. Magnuson, E. Tutuc, B. Yakobson, K. McCarty, Y. Zhang, P. Kim, J. Hone, L. Colombo and R. Ruoff, Science 342, (2013).

(25) J. Suk, A. Kitt, C. Magnuson, Y. Hao, S. Ahmed, J. An, A. Swan, B. Goldberg and R. Ruoff, ACS Nano 5, (2011).

(26) A. Pirkle, J. Chan, A. Venugopal, D. Hinojos, C. Magnuson, S. McDonnell, L. Colombo, E. Vogel, R. Ruoff and R. Wallace, Appl. Phys. Lett. 99, (2011).

(27) Y. Hao, Y. Wang, L. Wang, Z. Ni, Z. Wang, R. Wang, C. Koo, Z. Shen and J. Thong, Small 6, (2010).

(28) K. Alexandrou, N. Petrone, J. Hone and I. Kymissis, Appl. Phys. Lett. 106, (2015).

(29) J. Chen, C. Jang, S. Adam, M. Fuhrer, E. Williams and M. Ishigami, Nat Phys 4, (2008).

(30) A. Das, B. Chakraborty and A. Sood, Bulletin Of Materials Science 31, (2008).

(31) L. Malard, R. Moreira, D. Elias, F. Plentz, E. Alves and M. Pimenta, Journal Of Physics: Condensed Matter 22, (2010).

(32) E. Zhang, A. Newaz, B. Wang, C. Zhang, D. Fleetwood, K. Bolotin, R. Schrimpf, S. Pantelides and M. Alles, Appl. Phys. Lett. 101, (2012).

(33) Z. Kertesz and G. Parsons, Science 142, (1963).

(34) S. Subbarao, M. Bahlke and I. Kymissis, IEEE Trans. Electron Devices 57, (2010).

(35) D. Teweldebrhan and A. Balandin, Appl. Phys. Lett. 94, (2009).

(36) M. Kalbac, O. Lehtinen, A. Krasheninnikov and J. Keinonen, Adv. Mater. 25, (2012).

(37) E. Benton and E. Benton, Nuclear Instruments and Methods in Physics Research Section B: Beam Interactions with Materials and Atoms 184, (2001).

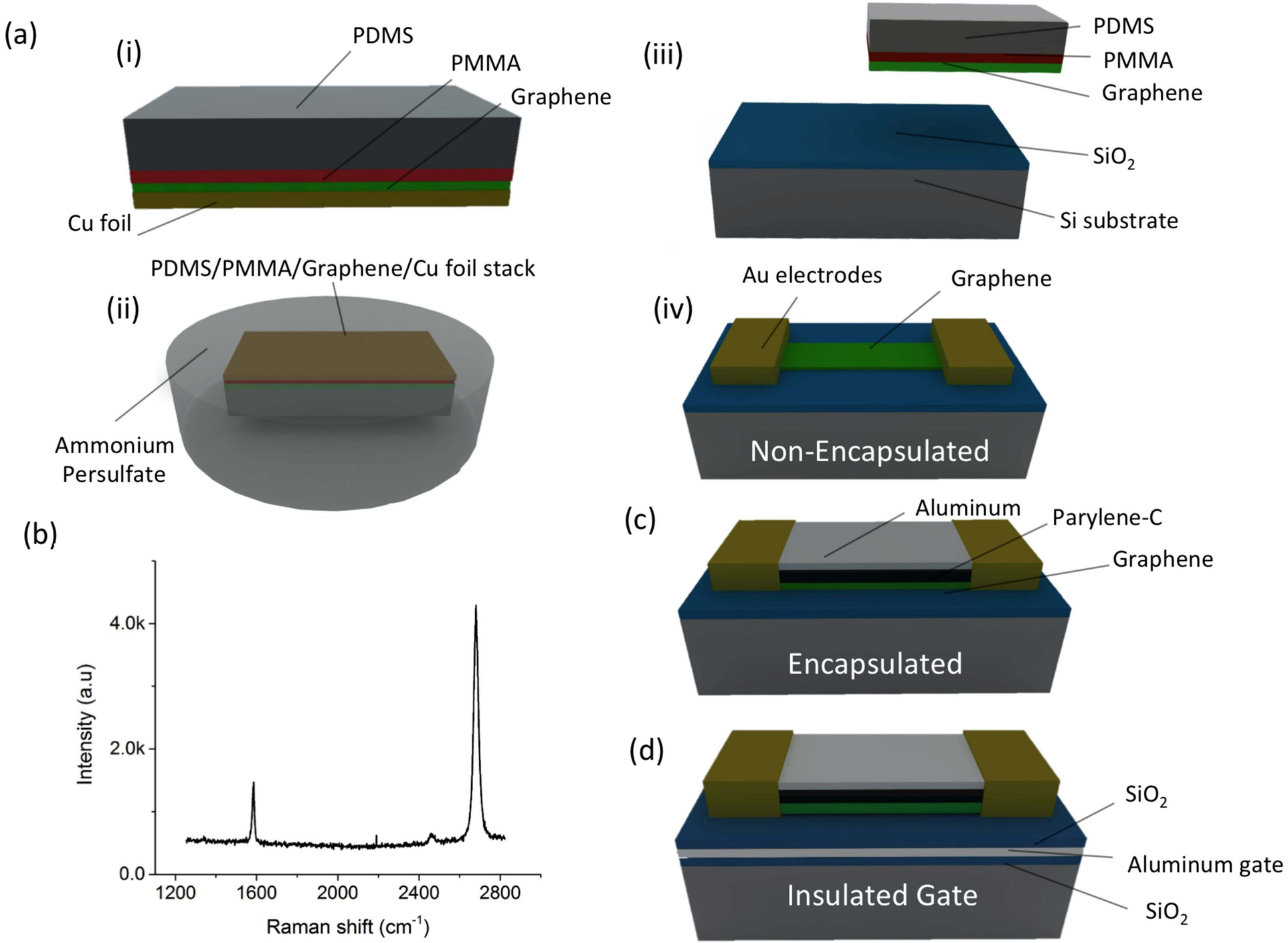
(a)
(i)
PDMS
PMMA
Graphene
Cu foil
PDMS/PMMA/Graphene/Cu foil stack
(ii)
Ammonium
Persulfate
(b)
Intensity (a.u)
4.0k
2.0k
0.0
1200
1600
2000
2400
2800
Raman shift (cm-1)
(iii)
PDMS
PMMA
Graphene
SiO2
Si substrate
(iv)
Au electrodes
Graphene
Non-Encapsulated
(c)
Aluminum
Parylene-C
Graphene
Encapsulated
(d)
SiO2
Aluminum gate
Insulated Gate
SiO2

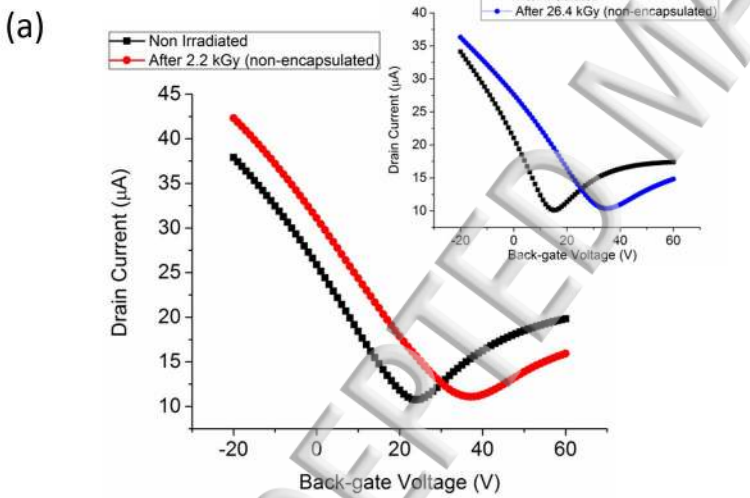

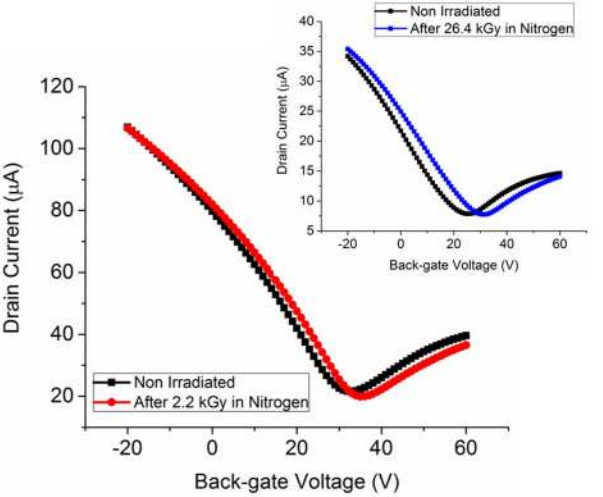

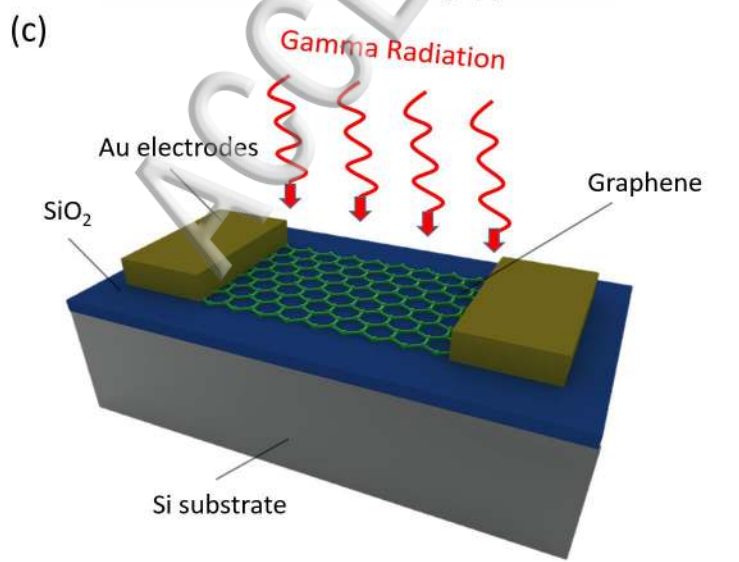

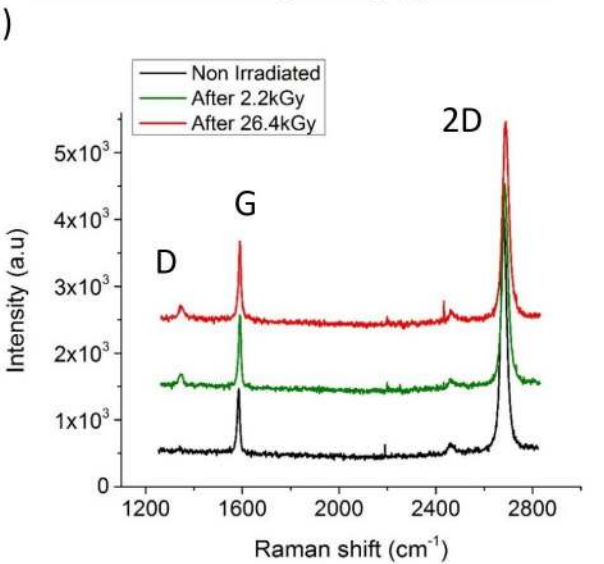

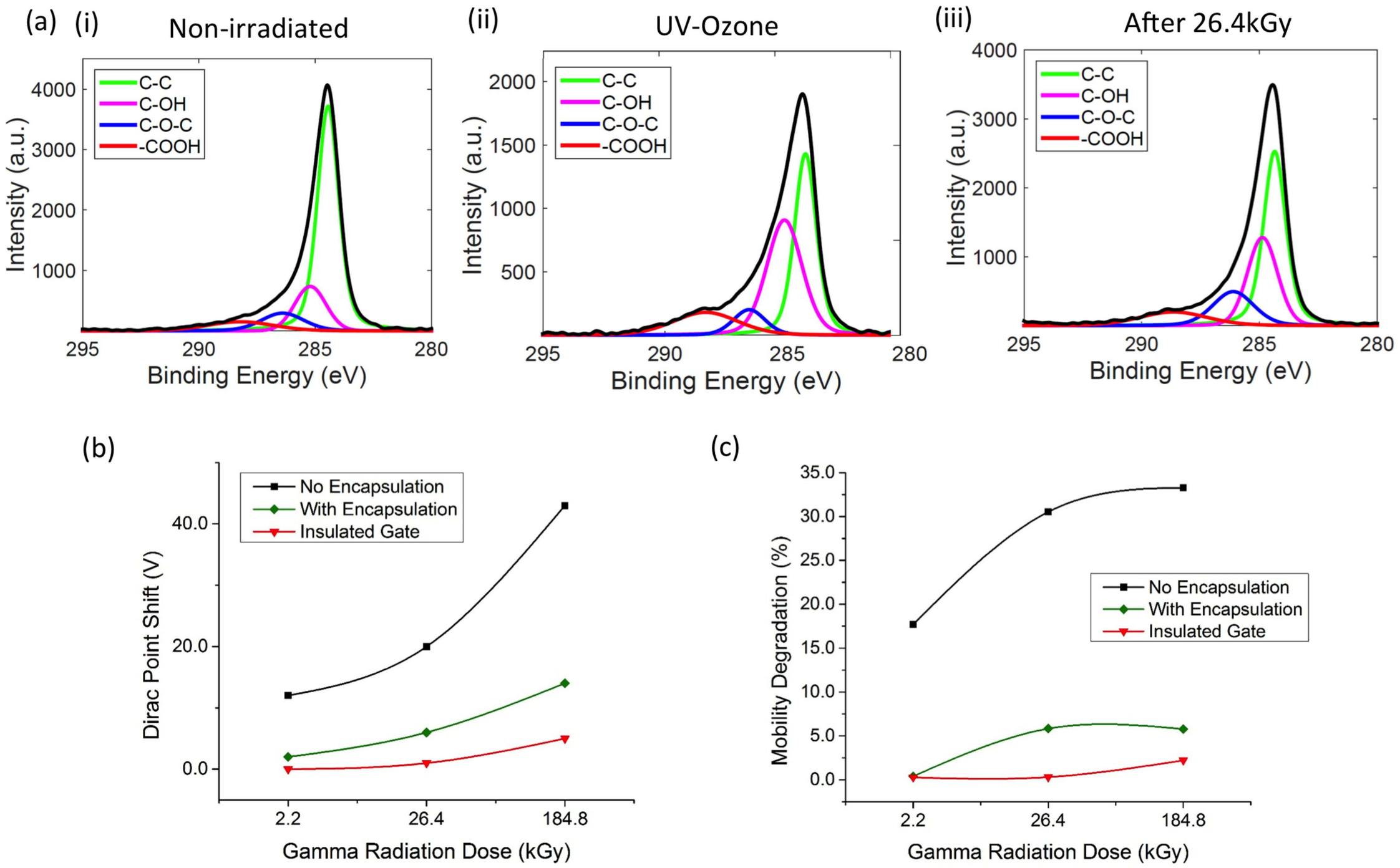
(a) (i) Non-irradiated
(ii) UV-Ozone
(iii) After 26.4kGy
C-C
C-OH
C-O-C
-COOH
Intensity (a.u.)
Binding Energy (eV)
295
290
285
280
(b)
No Encapsulation
With Encapsulation
Insulated Gate
Dirac Point Shift (V)
Gamma Radiation Dose (kGy)
2.2
26.4
184.8
(c)
Mobility Degradation (%)